

The 2dF Galaxy Redshift Survey: Voids and hierarchical scaling models

Darren J. Croton^{1,2}, Matthew Colless^{2,3}, Enrique Gaztañaga^{4,5}, Carlton M. Baugh⁶, Peder Norberg⁷, I. K. Baldry⁸, J. Bland-Hawthorn³, T. Bridges⁹, R. Cannon³, S. Cole⁶, C. Collins¹⁰, W. Couch¹¹, G. Dalton^{12,13}, R. De Propris², S. P. Driver², G. Efstathiou¹⁴, R. S. Ellis¹⁵, C. S. Frenk⁶, K. Glazebrook⁸, C. Jackson¹⁶, O. Lahav^{14,17}, I. Lewis¹², S. Lumsden¹⁸, S. Maddox¹⁹, D. Madgwick²⁰, J. A. Peacock²¹, B. A. Peterson², W. Sutherland²¹, K. Taylor¹⁵ (The 2dFGRS Team)

¹Max-Planck-Institut für Astrophysik, D-85740 Garching, Germany

²Research School of Astronomy & Astrophysics, The Australian National University, Weston Creek, ACT 2611, Australia

³Anglo-Australian Observatory, P.O. Box 296, Epping, NSW 2111, Australia

⁴INAOE, Astrofísica, Tonantzintla, Apdo Postal 216 y 51, Puebla 7200, Mexico

⁵Institut d'Estudis Espacials de Catalunya, ICE/CSIC, Edf. Nexus-104-c/Gran Capita 2-4, 08034 Barcelona, Spain

⁶Department of Physics, University of Durham, South Road, Durham DH1 3LE, UK

⁷ETHZ Institut für Astronomie, HPF G3.1, ETH Hönggerberg, CH-8093 Zürich, Switzerland

⁸Department of Physics & Astronomy, Johns Hopkins University, Baltimore, MD 21118-2686, USA

⁹Department of Physics, Queen's University, Kingston, Ontario K7L 3N6, Canada

¹⁰Astrophysics Research Institute, Liverpool John Moores University, Twelve Quays House, Birkenhead, L14 1LD, UK

¹¹Department of Astrophysics, University of New South Wales, Sydney, NSW 2052, Australia

¹²Department of Physics, University of Oxford, Keble Road, Oxford OX1 3RH, UK

¹³Space Science & Technology Division, Rutherford Appleton Laboratory, Chilton OX11 0QX, UK

¹⁴Institute of Astronomy, University of Cambridge, Madingley Road, Cambridge CB3 0HA, UK

¹⁵Department of Astronomy, California Institute of Technology, Pasadena, CA 91025, USA

¹⁶CSIRO Australia Telescope National Facility, PO Box 76, Epping, NSW 1710, Australia

¹⁷Department of Physics and Astronomy, University College London, Gower Street, London WC1E 6BT, UK

¹⁸Department of Physics, University of Leeds, Woodhouse Lane, Leeds, LS2 9JT, UK

¹⁹School of Physics & Astronomy, University of Nottingham, Nottingham NG7 2RD, UK

²⁰Department of Astronomy, University of California, Berkeley, CA 94720, USA

²¹Institute for Astronomy, University of Edinburgh, Royal Observatory, Blackford Hill, Edinburgh EH9 3HJ, UK.

Accepted —. Received —; in original form —

ABSTRACT

We measure the redshift space reduced void probability function (VPF) for 2dFGRS volume limited galaxy samples covering the absolute magnitude range $M_{b_j} - 5 \log_{10} h = -18$ to -22 . Theoretically, the VPF connects the distribution of voids to the moments of galaxy clustering of all orders, and can be used to discriminate clustering models in the weakly non-linear regime. The reduced VPF measured from the 2dFGRS is in excellent agreement with the paradigm of hierarchical scaling of the galaxy clustering moments. The accuracy of our measurement is such that we can rule out, at a very high significance, popular models for galaxy clustering, including the lognormal distribution. We demonstrate that the negative binomial model gives a very good approximation to the 2dFGRS data over a wide range of scales, out to at least $20h^{-1}\text{Mpc}$. Conversely, the reduced VPF for dark matter in a ΛCDM universe does appear to be lognormal on small scales but deviates significantly beyond $\sim 4h^{-1}\text{Mpc}$. We find little dependence of the 2dFGRS reduced VPF on galaxy luminosity. Our results hold independently in both the north and south Galactic pole survey regions.

Key words: galaxies: statistics, clustering; cosmology: theory, large-scale structure, voids.

1 INTRODUCTION

The galaxy distribution on the largest scales display striking geometrical features, such as walls, filaments and voids. These features contain a wealth of information about both the linear and non-linear evolution of galaxy clustering. The nature of such clustering is dependent on many large and small scale effects, such as the cosmological parameters, galaxy and cluster environmental effects and history, the underlying dark matter distribution, and the way in which the dark and luminous components of the Universe couple and evolve. By probing the lower and higher orders of galaxy clustering, one thus hopes to shed light on those physical processes on which the clustering is dependent.

The traditional tool used to analyse such distributions has been the 2-point correlation function (Davis & Peebles 1983, Davis et al. 1988, Fisher et al. 1994, Loveday et al. 1995, Norberg et al. 2001, Zehavi et al. 2002), providing a description of clustering at the lowest orders. However despite its usefulness, the 2-point correlation function only provides a full clustering description in the case of a Gaussian distribution. A more complete account of clustering must include correlation functions of higher orders, although these are often difficult to extract (see Croton et al. 2004 and Baugh et al. 2004 for an analysis of galaxy clustering in the 2dFGRS up to sixth order).

In light of this researchers have looked towards other clustering statistics to glean higher-order information from a galaxy distribution. Historically, many astronomers have favoured using void statistics (e.g. Fry 1986, Maurogordato & Lachize-Rey 1987, Balian & Schaeffer 1989, Fry et al. 1989, Bouchet et al. 1993, Gaztañaga & Yokoyama 1993, Vogeley et al. 1994). This approach is useful in that results are easily obtainable and are well supported by a solid theoretical framework (White 1979, Fry 1986, Balian & Schaeffer 1989), which directly relates the void distribution to that of galaxy clustering of higher orders.

In this paper we employ the completed 2dFGRS dataset to undertake a detailed analysis of the void distribution using the reduced void probability function. We rely heavily on the well established theoretical framework which connects the void distribution with galaxy clustering of all orders (Eq. 1 below). The distribution of voids and the moments of galaxy clustering of all orders are known to be intimately linked, and the study of one can reveal information about the other which would otherwise be difficult to measure. Our goal is thus to use the reduced void probability function to investigate if galaxy clustering in the 2dFGRS obeys a hierarchy of scaling, and on what physical scales this scaling holds. We explore a number of phenomenological models of galaxy clustering which exhibit hierarchical scaling, and use these models to help clarify the way in which higher-order clustering is constructed¹.

This paper is organised as follows. In Section 2 we give a brief review of the theory behind the void statistics to be employed in our analysis. In Section 3 we present the 2dFGRS data set, and in Section 4 the counts-in-cells method

we use to measure the void statistics is explained. Our results are presented in Section 5, and in Section 6 we provide a discussion and summary of our conclusions. Throughout, we adopt standard present day values of the cosmological parameters to compute comoving distance from redshift: a density parameter $\Omega_m = 0.3$ and a cosmological constant $\Omega_\Lambda = 0.7$.

2 VOID STATISTICS

2.1 The Void Probability Function

For a given distribution of galaxies, the count probability distribution function (CPDF), $P_N(V)$, is defined as the probability of finding exactly N galaxies in a cell of volume V randomly placed within the sample. In the case where $N = 0$ we have the void probability function (VPF), $P_0(V)$. A choice of spherical cells with which to sample the distribution makes P_0 a function of sphere radius R only. The VPF can be related to the hierarchy of p -point correlation functions by (White 1979):

$$P_0(R) = \exp \left[\sum_{p=1}^{\infty} \frac{(-\bar{N}(R))^p}{p!} \bar{\xi}_p(R) \right]. \quad (1)$$

Here \bar{N} is the average number of objects in a cell of volume V , and $\bar{\xi}_p$ is the p^{th} order correlation function averaged over V . A completely random (Poisson) distribution has $\xi_p \equiv 0$ for all $p > 1$, and thus P_0 reduces to a simple analytic expression:

$$P_{0P}(R) = \exp[-\bar{N}(R)]. \quad (2)$$

Any departure from this relation is therefore a signature of the presence of clustering.

2.2 Hierarchical Scaling

The idea that higher-order clustering arises in a *hierarchical* fashion from the 2-point correlation function appears naturally in perturbation theory and also in the highly non-linear regime of gravitational clustering (e.g. Peebles 1980), and is supported by much observational evidence (e.g. Maurogordato & Lachize-Rey 1987, Fry et al. 1989, Gaztañaga 1992, Bouchet et al. 1993, Bonometto et al. 1995, Benoist et al. 1999, see Bernardeau et al. 2002 for a review). The concept can be generalised by assuming that each p -point correlation function depends only on the product of the 2-point correlation function and a dimensionless scaling coefficient, S_p :

$$\bar{\xi}_p(R) = S_p \bar{\xi}^{p-1}(R), \quad (3)$$

where we have dropped the subscript 2 for the 2-point correlation function on the right-hand side for convenience (see Baugh et al. 2004 and Croton et al. 2004 for the measured values of S_p up to $p = 6$ in redshift space for the 2dFGRS).

The hierarchical idea is directly applicable to the VPF, which is itself dependent on an infinite sum of p -point correlation functions. The hierarchical assumption allows us to remove the higher-order correlation functions from Eq. 1:

$$P_0(R) = \exp \left[\sum_{p=1}^{\infty} \frac{(-\bar{N})^p}{p!} S_p \bar{\xi}^{p-1} \right]. \quad (4)$$

¹ Recently Hoyle et al. (2004) also measured the VPF of the 2dFGRS galaxy distribution, however their analysis focused more on the physical properties of voids in the 2dFGRS volume, rather than the hierarchical nature of galaxy clustering itself.

Furthermore, the above scaling relation allows us to express the VPF as a function of $\bar{N}\bar{\xi}$ only, where the scaling variable $\bar{N}\bar{\xi}$ approximately represents the average number of galaxies in a cell *in excess* of that expected given the mean density of the sample. We formalise this idea by firstly considering the analytic VPF expression for a purely random sample (Eq. 2). For the hierarchical situation, we can define a parameter χ with $P_0 = e^{-\bar{N}\chi}$, called the *reduced void probability function* (see Fry 1986):

$$\chi = -\ln(P_0) / \bar{N}. \quad (5)$$

We note here that, independent of the hierarchical assumption, χ normalises out the Poisson contribution to the distribution, and it is clear that the effects of clustering will appear as values of $\chi < 1$. Combining Eq. 4 and 5, the reduced VPF takes the form

$$\chi(\bar{N}\bar{\xi}) = \sum_{p=1}^{\infty} \frac{S_p}{p!} (-\bar{N}\bar{\xi})^{p-1}. \quad (6)$$

This exhibits the scaling advertised above, and the shape of $\chi(\bar{N}\bar{\xi})$ thus characterises the distribution of voids. If the scaling relation assumption holds, we expect different galaxy samples of different density and clustering strength to all collapse onto one universal curve, since all are a function of the same scaling variable. The curve will not be universal for different magnitude ranges if it turns out that the coefficients S_p are a strong function of galaxy magnitude. The values of S_p have recently been shown to depend at best only weakly on magnitude (see Croton et al. 2004).

In the hierarchical picture, when $\bar{N}\bar{\xi} \ll 1$ one always recovers the Poisson VPF, $\chi(\bar{N}\bar{\xi}) = 1$, regardless of the actual clustering pattern or its strength. In the regime where $\bar{N}\bar{\xi} < 1$ we see from Eq. 6 that the reduced void probability function is dominated by the Gaussian contribution: $1 - \frac{1}{2}\bar{N}\bar{\xi}$. Thus the interesting observational window, where we can separate different clustering models, comes for values of $\bar{N}\bar{\xi}$ larger than unity. In practice, this only seems to happen at scales R larger than a few h^{-1} Mpc, where $\bar{N} \sim R^3$ is large and dominates $\bar{\xi} \sim R^{-2}$. On smaller scales, where $\bar{\xi} > 1$, $\bar{N}\bar{\xi}$ will always be small, and galaxy samples will typically be too sparse to show measurable deviations from the Gaussian contribution. Thus, it should be stressed that the VPF is a good discriminant of weakly non-linear clustering only. In the highly non-linear regime voids do not provide us with much information.

Although the expansion given in Eq. 6 is technically only valid for small values of $\bar{N}\bar{\xi}$, the implications for clustering do extend beyond this. For large values of $\bar{N}\bar{\xi}$ models with different hierarchical amplitudes S_p give different reduced void probabilities χ : as $\bar{N}\bar{\xi}$ increases the value of χ gets smaller and the resulting VPF gets larger (with respect to the corresponding Poisson case). The Gaussian CPDF ($S_p = 0$) produces the smallest values of χ and therefore the largest deviations in the VPF. As we will illustrate with the models below, larger values of $S_p > 0$ will result in larger values of $\chi(\bar{N}\bar{\xi})$.

2.3 Phenomenological Models

In presenting our reduced VPF results, we follow the lead of Fry (1986) and Fry et al. (1989) and compare with a number

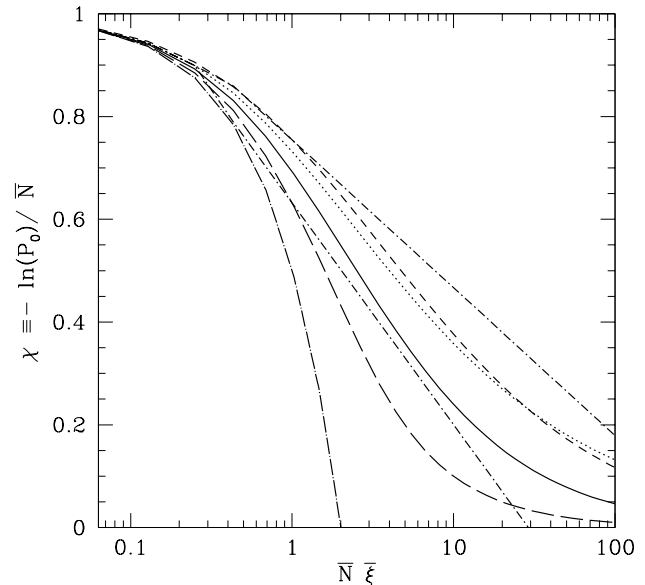


Figure 1. Reduced void probability χ for different models (left to right at $\chi \sim 0.4$): Gaussian (long-dashed-dotted, Eq. 12), minimal (long-dashed, Eq. 7), BBGKY (short-dashed-dotted, Eq. 10 with $Q = 2/3$), negative binomial (continuous, Eq. 8), thermodynamic (dotted, Eq. 9), lognormal (short-dashed) and BBGKY (short-dashed-dotted, Eq. 10 with $Q = 1$).

of model scaling relations that differ in the way they fix the scaling coefficients S_p . We give a brief description of these models here, and refer the reader to the cited papers and references therein for further details. In Fig. 1 we summarise the behaviour of each.

2.3.1 Minimal model

The first model is the so-called *minimal cluster model*, the motivation of which is to consider a clumpy galaxy distribution of clusters, the cluster distribution in space itself being Poisson with a Poisson galaxy occupancy. This is reminiscent of the halo model (e.g. Cooray & Sheth 2002) but with a Poisson halo/cluster profile. Evaluating the set of S_p 's from the distribution function generated by this model leads to a functional form for χ of

$$\begin{aligned} \chi &= (1 - e^{-\bar{N}\bar{\xi}}) / \bar{N}\bar{\xi} \quad (\text{minimal}), \\ S_p &= 1 \quad (\text{Skewness : } S_3 = 1). \end{aligned} \quad (7)$$

Fry (1986) speculated that this model represents a lower bound on the allowable functions $\chi(\bar{N}\bar{\xi})$ in any consistent hierarchical model.

2.3.2 Negative binomial model

The second model, commonly called the *negative binomial model*, has been used in a number of fields with different physical motivations (Klauder & Sudarshan 1968, Carruthers & Shin 1983, Carruthers & Minh 1983, Fry 1986, Elizalde & Gaztañaga 1992, Gaztañaga & Yokoyama 1993). After a set of T independent trials with probability q for “success” and $p = 1 - q$ for “failure”, the probability of having S number of successes and $F = T - S$

number of failures is given by the binomial distribution: $P(S) = (F + S)!/S!F!(1 - q)^F q^S$. The negative binomial distribution describes the probability for having S number of successes *after* a fixed number F of failures: $P(S) = (F + S - 1)!/S!(F - 1)!(1 - q)^F q^S$. Note that in the binomial case what is fixed is the total number of trials.

We can identify a “success” as finding a galaxy in a cell, so that $P_N = P(N = S)$ is the CPDF. The fixed number of failures, F , is assumed to be inversely proportional to $\bar{\xi}$ (the larger the $\bar{\xi}$, the smaller the number of failures to count a galaxy in a cell). The probability for a failure p is assumed to be proportional to the product $\bar{N}\bar{\xi}$ (because of clustering there is an $\bar{N}\bar{\xi}$ rms excess of galaxies within a cell with \bar{N} density: the larger this clumpiness the larger the probability to miss galaxies in a random cell). After fixing the proportionality constants, this leads to $F = 1/\bar{\xi}$ and $p = \bar{N}\bar{\xi}/(1 + \bar{N}\bar{\xi})$ (for a different derivation see Gaztañaga & Yokoyama 1993). This model is a discrete version of the gamma probability distribution (see Gaztañaga, Fosalba & Elizalde 2000). The reduced VPF and cumulants in this case are:

$$\begin{aligned}\chi &= \ln(1 + \bar{N}\bar{\xi})/\bar{N}\bar{\xi} \quad (\text{negative binomial}), \\ S_p &= (p - 1)! \quad (\text{Skewness : } S_3 = 2) .\end{aligned}\quad (8)$$

2.3.3 Thermodynamic model

The third model was first suggested by Saslaw and Hamilton (1984) and arose from a thermodynamic theory of the properties of gravitational clustering. The original model had a fixed degree of virialization (temperature or density variance) for all cell sizes, but such behaviour is inconsistent with observations. The model was later extended (see e.g. Fry 1986) to include a different level of virialization at each scale, to be identified with the variance $\bar{\xi}$ as a function of scale. The results is:

$$\begin{aligned}\chi &= [(1 + 2\bar{N}\bar{\xi})^{1/2} - 1]/\bar{N}\bar{\xi} \quad (\text{thermodynamic}), \\ S_p &= (2p - 3)!! \quad (\text{Skewness : } S_3 = 3) ,\end{aligned}\quad (9)$$

where $(2p - 3)!! = (2p - 3).(2p - 5).(2p - 7)...$ and truncates at zero.

2.3.4 Lognormal distribution

The *lognormal* distribution (e.g. Coles & Jones 1991, Weinberg & Cole 1993), is often used as a phenomenological model for galaxy and dark matter clustering. Although no analytic expression exists for the reduced void probability, it can be estimated numerically (see above references) and is found to behave similarly to the thermodynamic model, as shown in Fig. 1 (note how the dotted and the short-dashed lines overlap). As in the thermodynamic model, the lognormal distribution also has a large skewness: $S_3 = 3 + \bar{\xi}$ (which exactly tends to the thermodynamical value $S_3 \rightarrow 3$ on large scales where $\bar{\xi} \rightarrow 0$). In fact, it should be noted that the lognormal model is not truly hierarchical, as it does not have constant moments S_p , but in practice the variations have little effect on the reduced void distribution.

2.3.5 BBGKY model

The BBGKY model of Fry (1984) provides a prescription for χ and S_p as an asymptotic solution to the BBGKY kinetic equations:

$$\begin{aligned}\chi &= 1 - (\gamma + \ln 4Q\bar{N}\bar{\xi})/8Q \quad (\text{BBGKY}), \\ S_p &= (4Q)^{p-2} \frac{p}{2(p-1)} ,\end{aligned}\quad (10)$$

where $\gamma = 0.57721...$ is Euler’s constant. This asymptotic solution is only a good approximation for large values of $\bar{N}\bar{\xi}$. When $\bar{N}\bar{\xi}$ becomes small, for completeness we simply match it to the nearest model.

The skewness in the BBGKY model contains a free parameter, $S_3 = 3Q$, with the restriction that $Q > 1/3$. Fry (1984) used $Q \simeq 1$, which was close to the then observed $S_3 \simeq 3$ value measured from the 3-point function in real space (inferred from projected maps). Croton et al. (2004) and Baugh et al. (2004) have since shown that S_3 is in fact closer to $S_3 = 2$ in the 2dFGRS, corresponding to the case where $Q = 2/3$. Both possibilities are shown as short-dashed-dotted lines in Fig. 1, with the upper curve for $Q = 1$ and the lower curve for $Q = 2/3$. Since we later show that neither of these Q values with the BBGKY model are able to match the data very well, for the sake of clarity we omit the lower $Q = 2/3$ curve in subsequent figures. The upper curve is retained in order to demonstrate the range of possible χ values that a hierarchical model may have.

2.3.6 Poisson and Gaussian distributions

In addition to the above models we also use the analytic expressions of the reduced VPF for purely Poisson and Gaussian distributions. Trivially, from Eq. 6 we see that

$$\chi = 1 \quad (\text{Poisson}), \quad (11)$$

and

$$\begin{aligned}\chi &= 1 - \frac{1}{2}\bar{N}\bar{\xi} \quad (\text{Gaussian}), \\ S_p &= 0 \quad (\text{Skewness : } S_3 = 0) .\end{aligned}\quad (12)$$

The later only makes sense for small values of $\bar{N}\bar{\xi}$, but note that even when the underlying distribution is not Gaussian, the above expression always gives a good approximation to the void probability in the limit of small $\bar{N}\bar{\xi}$.

3 THE DATA SETS

3.1 The 2dFGRS Data Set

In our analysis we use the completed 2dFGRS (Colless et al. 2003). The catalogue is sourced from a revised and extended version of the APM galaxy catalogue (Maddox et al. 1990), and the targets are galaxies with extinction-corrected magnitudes brighter than $b_J = 19.45$. Our galaxy sample contains a total of 221,414 high quality redshifts. The median depth of the full survey, to a nominal magnitude limit of $b_J \approx 19.45$, is $z \approx 0.11$. We consider the two large contiguous survey regions, one in the south Galactic pole (SGP) and one towards the north Galactic pole (NGP), and restrict our attention to the parts of the survey with high redshift completeness ($> 70\%$). Full details of the 2dFGRS

Table 1. Properties of the combined 2dFGRS SGP and NGP volume limited catalogues (VLCs). Columns 1 and 2 give the faint and bright absolute magnitude limits that define the sample. Column 3 gives the median magnitude of the sample, computed using the Schechter function parameters quoted by Norberg et al. (2002). Columns 4, 5 and 6 give the number of galaxies, the mean number density and the mean inter-galaxy separation for each VLC, respectively. Columns 7 and 8 state the redshift boundaries of each sample for the nominal apparent magnitude limits of the survey; columns 9 and 10 give the corresponding comoving distances. Finally, column 11 gives the combined SGP and NGP volume. All distances are comoving and are calculated assuming standard cosmological parameters ($\Omega_m = 0.3$ and $\Omega_\Lambda = 0.7$).

Mag. range		Median mag.	N_G	ρ_{ave}	d_{mean}	z_{min}	z_{max}	D_{min}	D_{max}	Volume
$M_{b_J} - 5 \log_{10} h$		$M_{b_J} - 5 \log_{10} h$		$10^{-3}/h^{-3} \text{Mpc}^3$	$h^{-1} \text{Mpc}$			$h^{-1} \text{Mpc}$	$h^{-1} \text{Mpc}$	$10^6 h^{-3} \text{Mpc}^3$
-18.0	-19.0	-18.44	23290	9.26	4.76	0.014	0.088	39.0	255.6	2.52
-19.0	-20.0	-19.39	44931	5.64	5.62	0.021	0.130	61.1	375.6	7.97
-20.0	-21.0	-20.28	33997	1.46	8.82	0.033	0.188	95.1	537.2	23.3
-21.0	-22.0	-21.16	6895	0.110	20.9	0.050	0.266	146.4	747.9	62.8

and the construction and use of the mask quantifying the completeness of the survey can be found in Colless et al. (2001, 2003).

A model accounting for the change in galaxy magnitude due to redshifting of the b_J -filter bandpass (k-correction) and galaxy evolution (e-correction) was adopted following Norberg et al. (2002):

$$k(z) + e(z) = \frac{z + 6z^2}{1 + 20z^3} . \quad (13)$$

This model gives the mean k+e-correction over the mix of different spectral types observed in the 2dFGRS sample, and was shown by Norberg et al. to accurately account for such observational effects when estimating 2dFGRS galaxy absolute magnitudes.

3.2 Volume Limited Catalogues

The 2dFGRS galaxy catalogue is *magnitude-limited*, meaning the survey is constructed by observing galaxies brighter than the fixed apparent magnitude limit of $b_J=19.45$. A magnitude-limited galaxy catalogue is not uniform in space, since intrinsically fainter objects may be missed even if they are relatively nearby, while the most luminous galaxies will be seen out to large distances. This non-uniformity of the magnitude-limited catalogue must be dealt with for a correct statistical analysis, and the simplest way to do this with a catalogue the size of the 2dFGRS is by constructing a volume limited catalogue (VLC) from the magnitude-limited sample.

Volume limited catalogues are defined by choosing minimum and maximum *absolute* magnitude limits. These limits, along with the intrinsic apparent magnitude limits of the survey, define minimum and maximum redshift boundaries via standard luminosity–distance relations (Peebles 1980). The VLC is built by selecting galaxies whose redshift lies within the minimum and maximum boundaries just determined, and whose absolute magnitude lies within the specified absolute magnitude limits. Such galaxies can be displaced to any redshift within the VLC volume and still remain within the bright and faint apparent magnitude limits of the magnitude limited survey. Table 1 presents the properties of the combined NGP and SGP volume limited catalogues used in this paper.

4 MEASURING THE GALAXY DISTRIBUTION

To measure the void probability function we use the method of counts-in-cells. The survey volume is uniformly sampled with a large number (2.5×10^7) of randomly placed spheres of fixed radius R , and we record the number of times a sphere contains exactly N galaxies. Our choice of massive oversampling ensures a high level of statistical accuracy in the calculation (Szapudi 1998). The CPDF can then be found as the probability of finding exactly N galaxies in a randomly placed sphere:

$$P_N(R) = \frac{N_N}{N_T} , \quad (14)$$

where N_N is the number of spheres that contain exactly N galaxies out of the total number of spheres thrown down, N_T . By definition, the void probability function is the probability of finding an empty sphere:

$$P_0(R) = \frac{N_0}{N_T} . \quad (15)$$

The mean number of galaxies expected inside a sphere of radius R is readily calculated from

$$\bar{N}(R) = \sum N P_N(R) , \quad (16)$$

and this estimation of \bar{N} for each individual VLC is found to be independent of scale and indistinguishable from that determined from the known mean galaxy density. The volume averaged 2-point correlation function, $\bar{\xi}_2$, is found directly from the second moment of the CPDF:

$$\bar{\xi}_2(R) = \frac{\langle (N - \bar{N})^2 \rangle - \bar{N}(R)}{\bar{N}(R)^2} . \quad (17)$$

We have also carried out an independent counts-in-cells analysis by placing the spheres at the positions of a regular spatial lattice that homogeneously oversamples the survey area. The results are insensitive to these details.

The 2dFGRS has an inherent spectroscopic galaxy incompleteness which will change the results of any void analysis (Colless et al. 2001). In addition, due to the irregular geometry of the survey boundaries it is difficult to guarantee that every sphere will be completely contained within the regions we wish to measure. Since the CPDF is sensitive to such effects we adopt a technique which accurately accounts for such deficiencies. This method is explained and tested in Appendix A (see also Croton et al. 2004).

4.1 Error Estimation

We estimate the error on our void statistics using the set of 22 mock 2dFGRS surveys described by Norberg et al. (2002; see also Cole et al. 1998). These mock catalogues have the same radial and angular selection function as the 2dFGRS and have been convolved with the completeness mask of the survey. The mock catalogues are drawn from the Virgo Consortium’s Λ CDM Hubble Volume simulation and thus include sample variance due to large scale structure (see Evrard et al. 2002 for a description of the Hubble Volume simulation). The 1σ errors we quote correspond to the *rms* scatter over the ensemble of mocks (see Norberg et al. 2001). We have compared this estimate with an internal estimate using a jack knife technique (Zehavi et al. 2002). In the jack knife approach, the survey is split into subsamples. The error is then the scatter between the measurements when each subsample is omitted in turn from the analysis. The jack knife gives comparable errors to the mock ensemble for the VPF measurement.

5 RESULTS

We begin with Fig. 2, where we plot the reduced void probability function, χ , individually as a function of both the mean galaxy number, \bar{N} , and the variance, $\bar{\xi}$, in the top and bottom panels respectively. The physical scale given on each top axis corresponds to values for the $-20 > M_{b_J} - 5 \log_{10} > -21$ VLC only, and is included for reference (for VLCs of different mean density the scale at which a given \bar{N} or $\bar{\xi}$ will occur will be different). Note that for VLCs fainter than our reference this scale shifts to the right in the top panel and to the left in the bottom panel. The converse is true when considering brighter galaxies than the reference.

The main feature of this figure is that neither \bar{N} nor $\bar{\xi}$ individually show hierarchical scaling when plotted against χ . Note that smaller values of χ correspond to larger deviations from a Poisson distribution. Brighter galaxy samples show behaviour which is closer to that of the Poisson distribution for any given value of \bar{N} or $\bar{\xi}$, however this merely reflects the fact that the brightest VLCs are also the sparsest (Table 1).

We now test for hierarchical scaling in the 2dFGRS, as outlined in Section 2.2. In Fig. 3 we plot the reduced void probability function, χ , as a function of the scaling variable $\bar{N}\bar{\xi}$. In this way we eliminate the dependence of the void probability on the variance and mean density. This figure shows VLCs ranging in absolute magnitude from -18 to -22 . If a scaling between correlation functions of different orders exists we expect to see all points for each catalogue fall onto the same line. Again we provide a reference scale on the top axis, given for the $-20 > M_{b_J} - 5 \log_{10} > -21$ VLC, and note that for fainter galaxy samples this scale shifts to the right and conversely for brighter samples. Over-plotted are the scaling models previously discussed in Section 2.3: (bottom to top) the Gaussian (Eq. 12), minimal (Eq. 7), negative binomial (Eq. 8), thermodynamic (Eq. 9), lognormal, and BBGKY (Eq. 10, $Q = 1$) models respectively.

Fig. 3 demonstrates the clear signature of hierarchical scaling in the clustering moments of the 2dFGRS. All points

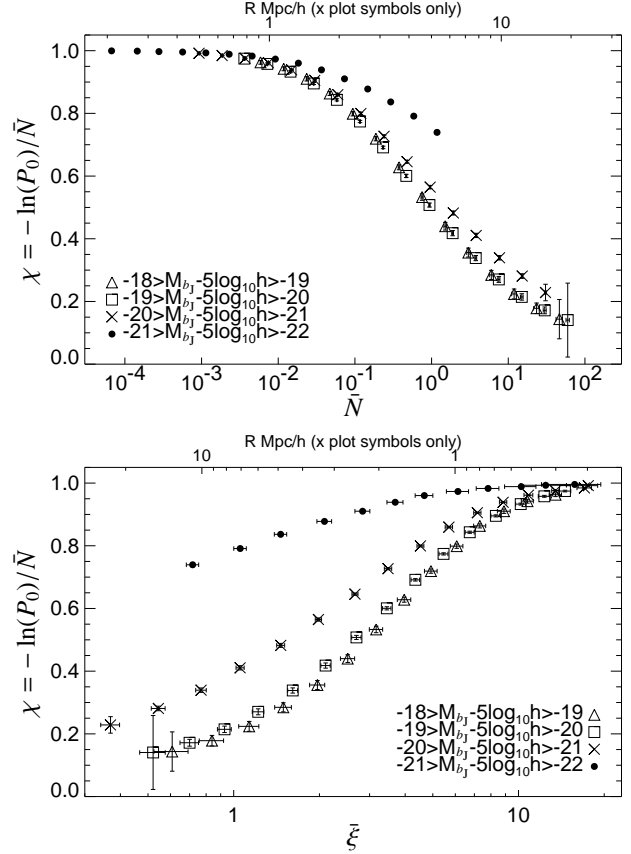


Figure 2. The 2dFGRS reduced VPF, $\chi = -\ln P_0/\bar{N}$, as a function of (top) the mean galaxy number, \bar{N} , and (bottom) the variance of the distribution, $\bar{\xi}$, as measured for volume limited catalogues in varying luminosity bins (Table 1). Smaller values of χ imply larger deviations from a Poisson distribution. The reference scale given on the top axis is for the $-20 > M_{b_J} - 5 \log_{10} > -21$ VLC only (each \bar{N} and $\bar{\xi}$ value individually correspond to different scales for each VLC). Notice that neither variable displays hierarchical scaling when plotted individually against χ .

are seen to follow a tight path (within the error bars) out to values of $\bar{N}\bar{\xi} \sim 30$, and sit close to the negative binomial model prediction along this entire range. Such values encompass galaxy clustering from the deeply non-linear to the linear regime, revealing hierarchical scaling out to scales of $\sim 20h^{-1}\text{Mpc}$ or more.

For comparison, in Fig. 3 we also present the dark matter reduced VPF measured from the Λ CDM Hubble volume simulation (particle mass $2.3 \times 10^{12}h^{-1}M_\odot$) (Evrard et al. 2002). We independently analyse 100 randomly placed cubes of side length $200h^{-1}\text{Mpc}$ (approximately equal in volume to our M^* galaxy volume limited sample), from which the rms is then plotted. In contrast to the 2dFGRS galaxies, the dark matter follows a lognormal distribution out to values of $\bar{N}\bar{\xi} \sim 6$ (a scale of approximately $R \sim 4h^{-1}\text{Mpc}$ in the simulation), but then deviates strongly on larger scales (the last point plotted corresponds to $R = 10h^{-1}\text{Mpc}$ in the simulation).

To highlight the differences between the 2dFGRS galaxy reduced VPF and the negative binomial prediction, in Fig. 4 we show the fractional difference between the two. Also included are the “bounding” models closest to the negative

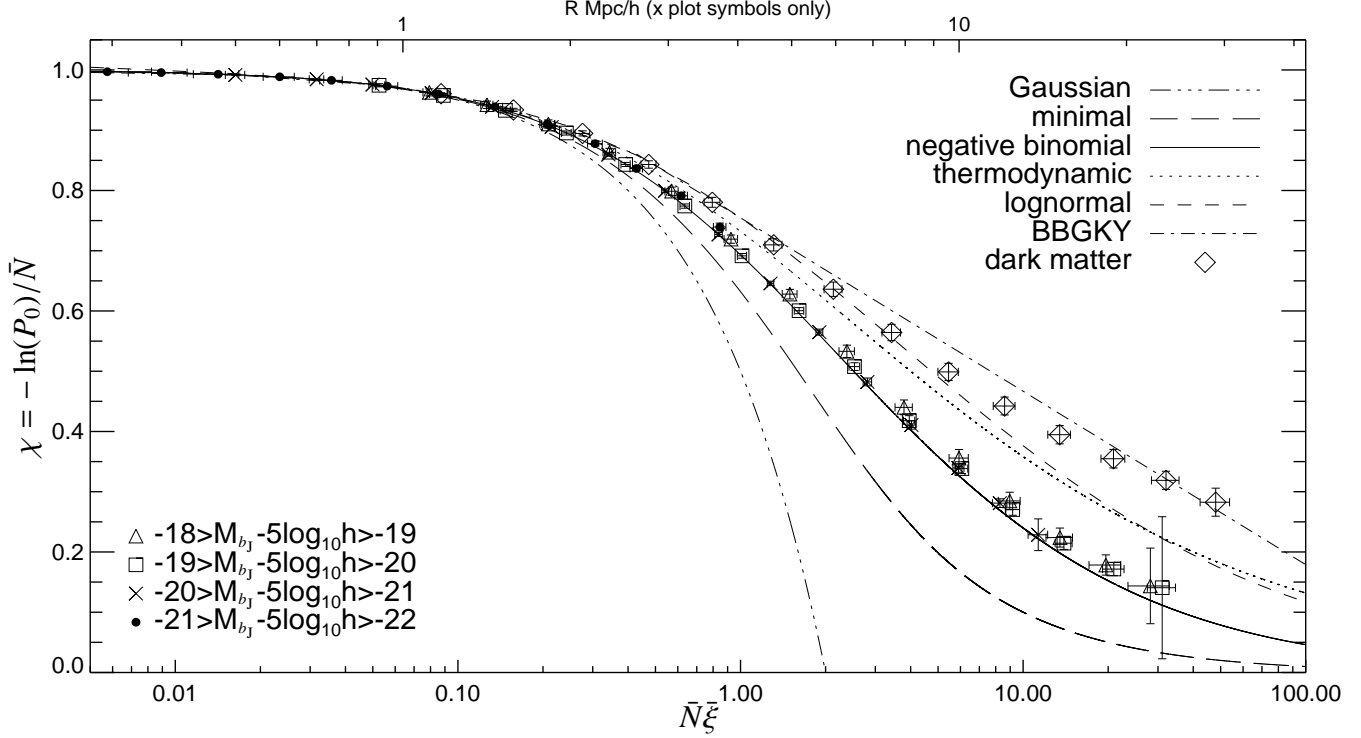


Figure 3. The reduced VPF, $\chi = -\ln P_0/\bar{N}$, as a function of the scaling variable $\bar{N}\bar{\xi}$ for the four 2dFGRS galaxy VLCs from Table 1. The dark matter reduced VPF, as measured from the Λ CDM Hubble Volume simulation, is shown as large diamonds. In all cases, smaller values of χ imply larger deviations from a Poisson distribution. The reference scale given on the top axis is for the $-20 > M_{b_J} - 5\log_{10} h > -21$ VLC only (each $\bar{N}\bar{\xi}$ value corresponds to a different scale for each VLC). If hierarchical scaling is present in the galaxy distribution all points should collapse onto a single line, which is clearly seen. The six curves represent the hierarchical models discussed in Section 2.3 (Eq. 7 to 12).

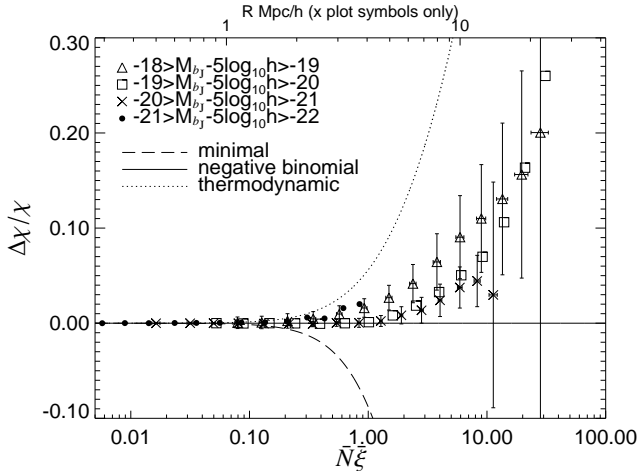


Figure 4. The fractional difference between the negative binomial model and the 2dFGRS, thermodynamic, and minimal reduced VPFs. The reference scale given on the top axis is for the $-20 > M_{b_J} - 5\log_{10} h > -21$ VLC only (each $\bar{N}\bar{\xi}$ value corresponds to a different scale for each VLC). Some error bars have been omitted for clarity. All 2dFGRS results are consistent with the negative binomial model at the 2σ level.

binomial: the minimal and thermodynamic models. All 2dFGRS points plotted are consistent with the negative binomial model at the 2σ level. At larger values of $\bar{N}\bar{\xi}$ we find

some small departures from the negative binomial model, and it is interesting to note that these deviations appear the greatest for the faintest VLC. This could be explained by the weak dependence of S_p on galaxy luminosity found by Croton et al. (2004), where fainter samples typically had larger S_p values than brighter samples (albeit with large error bars). The effect of such an increase in the hierarchical picture would result in a value of χ closer to unity (Eq. 6).

An important feature of Fig. 3 is the inconsistency of the reduced void probability function with a Gaussian distribution across all scales considered (up to approximately $30h^{-1}\text{Mpc}$). On large scales where the galaxy correlation functions become too small to measure independently, the value of \bar{N} is found to increase faster than $\bar{\xi}$ decreases, and thus χ is still affected strongly by higher-order correlations. It is clear that even in the quasi-linear regime, where one would expect galaxy clustering to be very simple, higher-order correlations still play a significant role in the make-up of the large scale distribution.

To evaluate the robustness of the results seen in Fig. 3 we apply two tests to illustrate the degree of confidence we should have in believing the existence of hierarchical scaling in the 2dFGRS. Firstly, one of the most valuable features of the 2dFGRS is that we have available data from two totally independent regions on the sky, the SGP and NGP. So far we have been calculating our void statistics from the combined volume of the two, but it is useful to check that the scaling properties still exist in the two regions indepen-

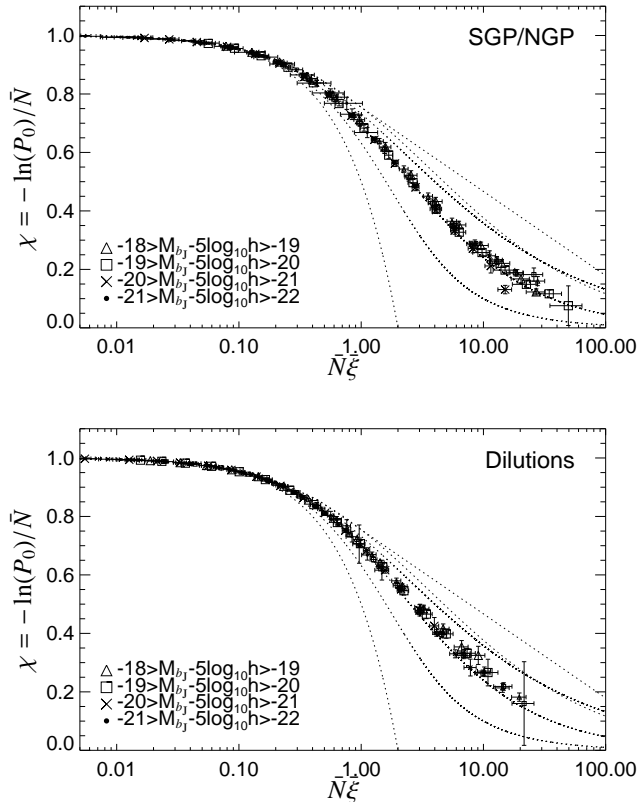


Figure 5. Two tests of the scaling properties seen in Fig. 3 using the reduced VPF, $\chi = -\ln P_0/\bar{N}$, as a function of the scaling variable $\bar{N}\xi$. (top) Independent SGP and NGP VLCs show identical scaling to that seen in Fig. 3. Here the large symbols represent the SGP result, and the small represent the NGP result. (bottom) The same combined VLCs as in Fig. 3, but now diluted by factors of 0.5 (large symbols) and 0.25 (small symbols). If hierarchical scaling exists in the galaxy distribution, dilution should make little difference to the results found in Fig. 3. For both panels, the dotted curves represent the same six models plotted in Fig. 3 and discussed in Section 2.3. Some error bars have been omitted for clarity.

dently. This we do in the top panel of Fig. 5, where the large symbols represent the SGP and small symbols the NGP. It is immediately clear that galaxies from both the SGP and NPG regions independently obey hierarchical scaling and reproduce the negative binomial results discussed previously to good accuracy.

Secondly, we test the scaling properties seen in Fig. 3 by calculating the reduced VPF for randomly diluted samples of galaxies. Such dilutions leave the 2-point correlation function unchanged, and within the hierarchical paradigm the scaling exhibited in Fig. 3 should also remain unchanged. This test is shown in the bottom panel of Fig. 5, where we have diluted each of the VLCs used in Fig. 3 by factors of 0.5 (large symbols) and 0.25 (small symbols). We again see that the trend for hierarchical scaling exists and follows the negative binomial model, consistent with our previous conclusions.

6 DISCUSSION

The 2dFGRS represents an enormous improvement in volume and number of galaxies over previous surveys, such as the CfA or the SSRS samples. Here we measure the galaxy distribution over both a wider range in variance ($\xi \sim 0.3 - 20$) and mean galaxy number ($\bar{N} \sim 10^{-4} - 10^2$). The impact on the VPF can be seen by comparing Fig. 3 above to Fig. 7 in Gaztañaga & Yokoyama (1993), where the CfA and SSRS data can not discriminate between the negative binomial and the thermodynamical models. As shown here in Fig. 3 and 4, although the agreement is not always perfect, the negative binomial does much better, by far, than any of the other models considered in the literature. This includes the lognormal distribution, which is close to the thermodynamical model (Fig. 1) and is widely used as a phenomenological clustering model. These results are valid independently in the NGP and SGP regions of the survey, and do not change when we randomly dilute the galaxy samples (Fig. 5). The lognormal distribution does, however, appear to be a good representation for the distribution of dark matter on smaller scales (less than $\sim 4h^{-1}\text{Mpc}$), although not at larger scales. The differences between the galaxy and dark matter reduced VPFs can be understood by noting the differences between their higher-order volume-averaged correlation functions, as shown by Baugh et al. (2004).

The 2dFGRS reduced void probability function appears to behave differently from the one presented by Vogeley et al. (1994) for the CfA-1 and CfA-2 samples, which show more scatter with magnitude and values well above the negative binomial model (compare their Fig. 4 to our Fig. 3). Here we do not observe any significant departure from the scaling models on scales larger than $R \sim 8.5h^{-1}\text{Mpc}$ as they had previously found. In contrast, our results indicate hierarchical scaling exists in the galaxy distribution out to scales of at least $R \sim 20h^{-1}\text{Mpc}$.

Although some heuristic derivations exist for the negative binomial distribution (see section 2.3), we have not found a satisfactory physical explanation for the very good performance of this model. The value of the skewness for the negative binomial model, $S_3 = 2$, is quite close to the direct measurement in the 2dFGRS: $S_3 = 1.86 - 2.03$ (Baugh et al. 2004). Other phenomenological models, such as the thermodynamical or the lognormal distribution, have larger values for the skewness ($S_3 \simeq 3$). A similar trend was found by Baugh et al. for the higher order coefficients S_4 , S_5 , and S_6 . In this respect it is not totally surprising that the negative binomial does better. The one freedom the reduced VPF has is in the value of the scaling coefficients which appear in the sum in Eq. 6. If these coefficients are found to match that predicted by a particular hierarchical scaling model, then one would expect their reduced VPFs to look similar.

Perturbation theory with Gaussian initial conditions predict values for the S_p 's that are universal and only depend on the local spectral index. They are therefore a known function of scale. Such scale dependence, however, breaks the hierarchy in Eq. 3, and therefore the universality of the scaling in Eq. 6. On the other hand, redshift space distortions and biasing tend to wash away this scale dependence (see e.g. Fig. 49 in Bernardeau et al. 2002), an argument which has been used to explain the good performance of the scaling hierarchy. But, as shown by Baugh et al. (2004)

and Croton et al. (2004), the measured values of the S_p 's do not seem to match the expectations in either dark matter models or mock galaxy surveys (both in redshift space). The reasons for this, and a more physically motivated interpretation of the negative binomial model, will provide important constraints to be matched by models of galaxy formation.

ACKNOWLEDGEMENTS

We wish to thank everyone involved with the 2dF instrument and Anglo-Australian telescope for their sustained effort over many years in producing the 2dFGRS. Many thanks also go to Saleem Zaroubi, Simon White, and Andrew Benson. DC acknowledges the financial support of the Mount Stromlo Bok Honours Scholarship, the Australian National University Coombs Honours Scholarship, and the International Max Planck Research School in Astrophysics Ph.D. fellowship. EG acknowledges support from the Spanish Ministerio de Ciencia y Tecnologia, project AYA2002-00850 and EC FEDER funding. CMB is supported by a Royal Society University Research Fellowship. PN acknowledges receipt of a Zwicky Fellowship.

REFERENCES

- Balian R. & Schaeffer R. 1989, *A&A*, 220, 1
 Baugh C. et al. (2dFGRS team) 2004, *MNRAS*, submitted (astro-ph/0401405)
 Benoist C., Cappi A., da Costa L. N., Maurogordato S., Bouchet F. R., & Schaeffer R. 1999, *ApJ*, 514, 563
 Bernardeau F., Colombi S., Gaztanaga E., & Scoccimarro R. 2002, *PhysRep*, 367, 1
 Bonometto S. A., Borgani S., Ghigna S., Klypin A., & Primack J. R. 1995, *MNRAS*, 273, 101
 Bouchet F. R., Strauss M. A., Davis M., Fisher K. B., Yahil A., & Huchra J. P. 1993, *ApJ*, 417, 36
 Cole S., Hatton S., Weinberg D. H., & Frenk C. S. 1998, *MNRAS*, 300, 945
 Coles P. & Jones B. 1991, *MNRAS*, 248, 1
 Colless M. et al. (2dFGRS team) 2001, *MNRAS*, 328, 1039
 Colless M. et al. (2dFGRS team) 2003, astro-ph/0306581
 Croton D. et al. (2dFGRS team) 2004, *MNRAS*, submitted (astro-ph/0401434)
 Cooray A. & Sheth R. 2002, *Phys.Rep.* 372, 1
 Curruthers P., & Minn D. V. 1983, *Phys. Lett. B*, 131, 116
 Curruthers P., & Shih C. C. 1983, *Phys. Lett. B*, 127, 242
 Davis M. & Peebles P. J. E. 1983, *ApJ*, 267, 465
 Davis M., Meiksin A., Strauss M. A., da Costa L. N., & Yahil A. 1988, *ApJ*, 333, L9
 Efstathiou G., Kaiser N., Saunders W., Lawrence A., Rowan-Robinson M., Ellis R.S., Frenk C.S., 1990, *MNRAS*, 247, 10P
 Elizalde E. & Gaztanaga E. 1992, *MNRAS*, 254, 247
 Evrard A. E., et al. (Virgo Consortium) 2002, *ApJ*, 573, 7
 Fisher K. B., Davis M., Strauss M. A., Yahil A., & Huchra J. 1994, *MNRAS*, 266, 50
 Fry, J. N. 1984, *ApJ Lett*, 277, L5
 Fry J. N. 1986, *ApJ*, 306, 358
 Fry J. N., Giovanelli R., Haynes M. P., Melott A. L., & Scherrer R. J. 1989, *ApJ*, 340, 11
 Gaztañaga E. 1992 *ApJ*, 398, L17
 Gaztañaga E. & Yokoyama J. 1993, *ApJ*, 403, 450
 Gaztañaga E., Fosalba P., & Elizalde E. 2000 *ApJ*, 539, 522
 Hoyle F. & Vogeley M. S. 2004, *ApJ*, submitted (astro-ph/0312533)

- Klauder J. R. & Sudarshan E. C. G. 1968, *Fundamentals of Quantum Optics*, (New York:Benjamin)
 Loveday J., Maddox S. J., Efstathiou G., & Peterson B. A. 1995, *ApJ*, 442, 457
 Maddox S. J., Efstathiou G., & Sutherland W. J. 1990, *MNRAS*, 246, 433
 Maurogordato S. & Lachieze-Rey M. 1987, *ApJ*, 320, 13
 Norberg, P. et al. (2dFGRS team) 2001, *MNRAS*, 328, 64
 Norberg, P. et al. (2dFGRS team) 2002, *MNRAS*, 336, 907
 Peebles P. J. E. 1980, *The Large-Scale Structure of the Universe* (Princeton Univ Press)
 Saslaw W. C. & Hamilton A. J. S. 1984, *ApJ*, 276, 13
 Szapudi I. 1998, *ApJ*, 497, 16
 Vogeley M. S., Geller M. J., Park C., & Huchra J. P. 1994, *ApJ*, 108, 745
 White S. D. M. 1979, *MNRAS*, 186, 145
 Weinberg D.H., & Cole S. 1992, *MNRAS*, 259, 652
 Zehavi I. et al. (SDSS team) 2002, *ApJ*, 571, 172

APPENDIX A: CORRECTING FOR INCOMPLETENESS IN THE 2DFGRS

The 2dFGRS is spectroscopically incomplete to a small degree resulting in missed galaxies (see Colless et al. 2001), and some spheres used in our counts-in-cells analysis may straddle the survey boundaries or holes resulting in missed volume. Such influences will induce an artificial “voidness” that will be picked up by our VPF measurements, and any analysis that neglects these effects will tend to over predict the VPF. Thus it is desirable to devise a method with which one can confidently correct for such incompleteness. This is not a trivial exercise, since weighting schemes that work with other statistics (e.g. Efstathiou et al. 1990) cannot necessarily be applied here, as the VPF will remain uncorrected (how does one weight no galaxies?). Such techniques will lead to an under-estimation of the mean density of galaxies and an over-estimation of the influence of the voids. Ideally, we need to ensure that any correction faithfully reproduces the full CPDF of the complete distribution for all orders of galaxy clustering.

To resolve these problems we have adopted the following method. When a satisfactory sphere location is found in the 2dFGRS wedge we project the sphere onto the sky and estimate, using the survey masks (Colless et al. 2001), the average completeness f within the sphere. Due to the incompleteness effects described above we typically will have $f < 1$. Instead of viewing this incompleteness as missed galaxies, we instead consider it as *missed volume*, and to compensate we scale the radius of the sphere according to $R' = R/f^{1/3}$. This new radius gives an effective sphere volume *with incompleteness* equal to that of a 100% complete sphere with the original radius. Galaxies are counted within the new radius R' , but contribute their counts to the scale R . Each sphere we place is individually scaled in this way according to its local incompleteness, as given by the masks. We note that due to our chosen acceptable minimum incompleteness of 0.7 spheres are never scaled beyond the radius bin R under consideration. Thus each correction applies only to the value of the VPF at each radius point plotted.

We have tested the robustness of our method by comparing measurements of the CPDF using a fully sampled, complete Hubble Volume 2dFGRS mock VLC (Norberg et al. 2002) with those from the same mock but which have

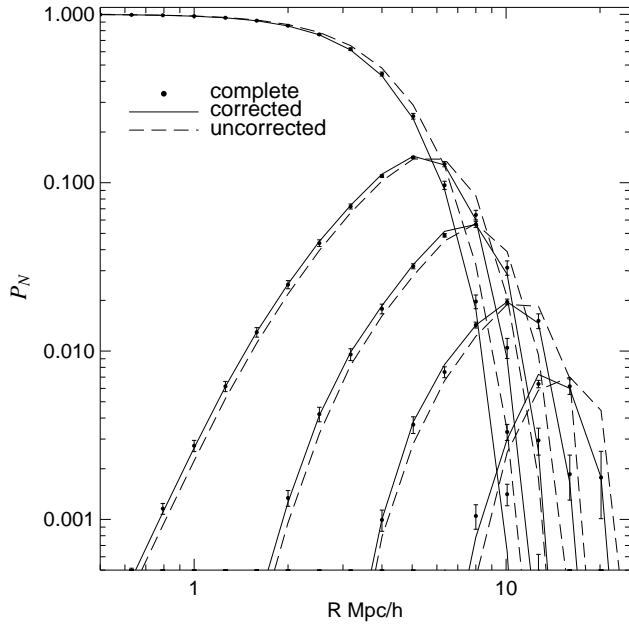


Figure 6. Correcting for incompleteness in the 2dFGRS. The CPDF, P_N , for a Hubble Volume 2dFGRS mock VLC in the magnitude range $-19 > M_{b,j} - 5 \log_{10} > -20$: left to right $N = 0$ (the VPF), 2, 6, 20 and 70. The points with errors represent the complete mock, the solid line is the corrected incomplete mock and the long-dashed line is the uncorrected incomplete mock. Note the uncorrected incomplete mock always lies outside the error bars.

been made artificially incomplete using the survey masks (spectroscopically, and including irregular boundaries and holes) and then corrected. In Fig. 6 we show the results for P_N vs. radius, where $N = 0$ (the VPF), 2, 6, 20 and 70 (note other N 's are omitted for clarity, but all behave similarly over the scales where the VPF is of interest to us). Here the points with error bars are the complete P_N 's, the solid lines are the equivalent corrected incomplete P_N 's, and the dashed lines represent the uncorrected incomplete P_N 's. As can be seen, the complete points and corrected lines are fully consistent, whereas the uncorrected values almost always lie off the complete points and well outside their error bars (note the steepness of each curve which is plotted on a log scale). The P_0 curve in particular demonstrates that such incompleteness effects must be accounted for to obtain correct void measurements; simply building volume limited catalogues is not enough and will lead to an over-prediction of the scale and frequency of voids in the survey. Our method can be applied to any counts-in-cells analysis where incompleteness in the galaxy distribution is present.